



CHORUS

This is the accepted manuscript made available via CHORUS. The article has been published as:

Phase transition systematics in BiVO_4 by means of high-pressure-high-temperature Raman experiments

J. Pellicer-Porres, D. Vázquez-Socorro, S. López-Moreno, A. Muñoz, P. Rodríguez-Hernández, D. Martínez-García, S. N. Achary, A. J. E. Rettie, and C. Buddie Mullins

Phys. Rev. B **98**, 214109 — Published 17 December 2018

DOI: [10.1103/PhysRevB.98.214109](https://doi.org/10.1103/PhysRevB.98.214109)

Phase transition systematics in $BiVO_4$ by means of high pressure-high temperature Raman experiments.

J. Pellicer-Porres^{a,*}, D. Vázquez-Socorro^a, S. López-Moreno^b, A. Muñoz^c, P. Rodríguez-Hernández^c,
D. Martínez García^a, S. N. Achary^d, A. J. E. Rettie^e, and C. Buddie Mullins^e

^aMALTA Consolider Team, ICMUV, Universidad de Valencia,

c/Dr. Moliner 50, 46100 Burjassot, Valencia, Spain

^bCONACYT - División de Materiales Avanzados, IPICYT,

Camino a la presa San José 20155, San Luis Potosí, S. L. P. 78216, Mexico

^cDepartamento de Física, Instituto de Materiales y Nanotecnología,

MALTA Consolider Team, Universidad de La Laguna, E-38205 La Laguna, Tenerife, Spain

^dChemistry Division, Bhabha Atomic Research Centre, Trombay, Mumbai 400085, India and

^eMcKetta Department of Chemical Engineering, The University of Texas at Austin, Austin, Texas 78712, United States

(Dated: November 13, 2018)

We report here high pressure-high temperature Raman experiments performed on $BiVO_4$. We have characterized the fergusonite and scheelite phases (powder and single crystal samples) and the zircon polymorph (nano powder). The experimental results are supported by ab-initio calculations, which in addition provide the vibrational patterns. The temperature and pressure behavior of the fergusonite lattice modes reflects the distortions associated with the ferroelastic instability. The linear coefficients of the zircon phase are in sharp contrast with the behavior observed in the fergusonite phase. The boundary of the fergusonite to scheelite second order phase transition is given by $T_{F-Sch}(K) = -166(8)P(GPa) + 528(5)$. The zircon to scheelite, irreversible, first order phase transition takes place at $T_{Z-Sch}(K) = -107(8)P(GPa) + 690(10)$. We found evidence of additional structural changes around 15.7 GPa, which in the downstroke were found to be not reversible. We have analyzed the anharmonic contribution to the wavenumber shift in fergusonite using an order parameter. The introduction of a critical temperature depending both on temperature and pressure allows description of the results of all the experiments in a unified way.

PACS numbers: xx

I. INTRODUCTION

Orthovanadate materials, with composition given by AVO_4 , where A is a trivalent metal or rare-earth ion, have a large number of technological applications.¹⁻⁷ $BiVO_4$, in particular, stirs special interest as a photocatalyst.⁸⁻¹⁰ The photocatalytic activity of $BiVO_4$ strongly depends on the crystalline phase and morphology,¹⁰ with nanoparticles being of particular interest.

AVO_4 compounds mostly crystallize^{11,12} in the zircon structure (Z, S. G. 141, $I4_1/amd$). Under high pressure, orthovanadates with light rare earth cations (larger radii) transform to a monazite type polymorph (M, S. G. 14, $P2_1/n$).¹³⁻¹⁷ However, zircon type compounds with a small rare-earth cation present an irreversible transition to the scheelite phase (S, S. G. 88, $I4_1/a$) and a second transition to the fergusonite (F, S. G. 15, $I2/b$) at higher pressures.^{15,18-20}

In $BiVO_4$ the general scheme followed by orthovanadates is altered. $BiVO_4$ can be prepared with the zircon structure,^{21,22} but this phase is only metastable. Given the small radii of Bi compared to rare earth elements, the scheelite phase could be expected to be the stable phase. However, the thermodynamically stable polymorph of $BiVO_4$ at ambient conditions is fergusonite.²³ It appears that the monoclinic symmetry of the fergusonite phase is the result of a distortion of the tetragonal symmetry of the scheelite phase^{23,24} by a ferroelastic instability.²⁵

Opposite to other orthovanadates, a second order phase transition from the fergusonite to the scheelite phase is observed either at high pressure²⁶⁻²⁸ [1.4(1) GPa] or high temperature^{23,28-35} [525(3) K]. Another approach to stabilize the tetragonal scheelite phase is appropriate doping of the sample.³⁶⁻³⁸ Additionally, the compound is found in nature with an orthorhombic structure called pucherite (S. G. 60, $Pnca$).³⁹

Previous^{26,30} Raman scattering experiments in the scheelite/fergusonite phases were focused on the lowest optical modes at the center of the Brillouin zone, which on the tetragonal paraelastic phase has B_g symmetry. The coupling of this mode with a the ferroelastic distortion was suggested as the driving mechanism for the transition. Subsequent Brillouin experiments^{31,32} demonstrated the existence of a soft acoustic mode and supported the proper character of the ferroelastic phase transition. The analysis of the angular dependence of the sound waves revealed³¹ perfect softening of the transversal acoustic branch along a direction in the tetragonal (001) plane. Inelastic neutron scattering³³ characterized the softening of the transversal acoustic branch along $[0.7\xi, \xi, 0]$. The dispersion curve showed an upward curvature which could not be completely determined, thus limiting the conclusions extracted about the associated elastic constant, which did not manifest complete softening.

In this work we complement previous Raman experiments describing the behavior of the whole set of Raman

active modes as well as extending the pressure range and introducing simultaneously high pressure-high temperature conditions. The scheelite phase is destabilized at 15.7 GPa. The high pressure behavior of zircon will be discussed for the first time. The experimental findings are supported by *ab-initio* calculations, which in addition provide the vibrational pattern. Finally, we use the Landau theory to discuss the full set of high pressure-high temperature experiments. The paper is organized as follows. In Sec. IV A the ambient conditions results are described, including the characterization of the modes in terms of symmetry, vibration patterns and relationships between the three phases. Sec. IV B is devoted to high-pressure and high temperature results, beginning with a description of pressure and temperature coefficients, then describing the phase boundaries and finally analyzing how the anharmonic interactions affect the wavenumber shifts in the fergusonite structure.

II. EXPERIMENTAL

The $BiVO_4$ samples used in the Raman experiments had different origins. Single crystals adopting the fergusonite structure were grown by the floating zone technique.^{40,41} Zircon $BiVO_4$ is prepared by a precipitation method from acidic aqueous solution of $Bi(NO_3)_3$ and NH_4VO_3 at room temperature.⁴² Polycrystalline fergusonite in powder form was purchased from Alfa-Aesar (CAS 14059-33-7, 99.9% purity).

High pressure Raman measurements were performed using a diamond anvil cell having a 16:3:1 methanol-ethanol-water mixture or Ne as pressure-transmitting medium.⁴³ The sample was loaded into a cylindrical pressure chamber with a diameter of 100-200 μm and a thickness between 40 and 50 μm , which was holed in the center of the stainless steel gasket. Pressure was determined using ruby luminescence.⁴⁴ Raman spectra were collected in the backscattering geometry using a 632.8 nm He-Ne laser and a Jobin-Yvon spectrometer in combination with a thermoelectric-cooled multichannel CCD detector with spectral resolution around 2 cm^{-1} . A laser power of less than 2 mW before the diamond anvil cell was necessary in order to avoid the fergusonite to scheelite phase transition induced by sample heating. High temperature experiments at ambient pressure were conducted in an air atmosphere. Temperature was measured via Pt resistance. High pressure-high temperature experiments were carried out employing external heating. Temperature was established by the calibrated reading of a thermocouple in close contact with the diamonds. In this set-up, pressure was determined using the fluorescence line of $SrB_4O_7 : Sm^{2+}$.⁴⁵

III. CALCULATIONS

Calculations of the total energy were performed within the framework of the density functional theory (DFT)⁴⁶ and the projector-augmented wave (PAW)^{47,48} method as implemented in the Vienna Ab initio Simulation Package (VASP).⁴⁹⁻⁵² A plane-wave energy cutoff of 600 eV was used to ensure a high precision in our calculations. The exchange-correlation energy was described with the HSE06 hybrid functional.⁵³⁻⁵⁶ This functional has been used with success in the study of other vanadates such as $InVO_4$ and $FeVO_4$.^{57,58} The Monkhorst-Pack scheme⁵⁹ was employed to discretize the Brillouin zone (BZ) integrations with meshes $3 \times 3 \times 3$, $4 \times 4 \times 2$, and $3 \times 2 \times 4$, which correspond to a set of 6, 4, and 6, special k-points in the irreducible BZ for the zircon, scheelite, and fergusonite phases, respectively. In the relaxed equilibrium configuration, the forces are less than 2 $meV/\text{\AA}$ per atom in each of the Cartesian directions. This high degree of convergence is required for the calculations of vibrational properties using the direct force constant approach.⁶⁰ High-pressure lattice dynamic calculations were carried out at the zone center (Γ point) of the BZ.

IV. RESULTS AND DISCUSSION

A. Raman in ambient conditions

1. Mode characterization

We begin our description with the fergusonite phase. A group symmetry analysis yields eighteen Raman active modes:

$$\Gamma_R(F) = 8A_g + 10B_g \quad (1)$$

A_g (B_g) modes are symmetrical (antisymmetrical) with respect to the twofold c -axis. The Raman tensors of the modes are:

$$R_{A_g} = \begin{pmatrix} a & d & 0 \\ d & b & 0 \\ 0 & 0 & c \end{pmatrix} \quad R_{B_g} = \begin{pmatrix} 0 & 0 & e \\ 0 & 0 & f \\ e & f & 0 \end{pmatrix} \quad (2)$$

Our single crystals have their largest surface oriented perpendicular to the c -axis. When using single crystals we have only access to A_g modes. In the experiments with the sample in powder form all the modes are allowed. A key to the identification of B_g modes has been its observation in powder spectra but not in single crystals (Fig. 1). Tab. I presents a summary of the results. We include the wavenumbers and symmetries yielded by the *ab-initio* calculations performed with the hybrid functional *HSE06*, as well as the results corresponding to the single crystal study reported in Ref. 34. The B_g^1 , B_g^2 and A_g^1 modes are too low in energy to be accessible in our

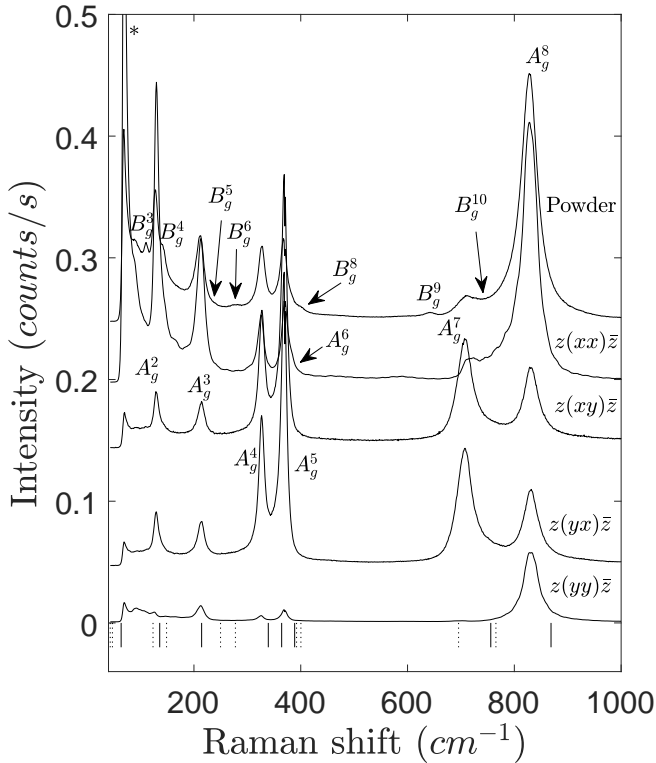


FIG. 1: Symmetry assignment of Raman modes in the fergusonite phase by comparison of single crystal polarized spectra with the spectrum of the sample in powder form. In single crystal spectra B_g modes are not allowed. The spectra have been shifted for clarity. Continuous (dashed) lines at the bottom correspond to the *ab initio* calculation for the A_g (B_g) modes. The peak labelled with a star is a glitch originated by the edge filter.

Raman set-up (edge filter cutoff around 70 cm^{-1}). The B_g^5 mode at $241(1) \text{ cm}^{-1}$ is very weak. It was not reported in Ref. 34. Its identification is supported by *ab initio* computations. The agreement between experiment and theory is in general satisfactory, though it is worse for the highest energetic modes. From the experimental point of view the identification of the B_g^9 , A_g^7 and A_g^8 modes is straightforward. Although the presence of the B_g^{10} mode is clear, its precise wavenumber characterization is troublesome due to the nearby presence of strong modes.

The Raman active modes in the scheelite phase are given by:

$$\Gamma_R(S) = 3A_g + 5B_g + 5E_g \quad (3)$$

The scheelite phase is not stable in ambient conditions. The spectra obtained at either high pressure or high temperature are presented in Fig.2. In order to compare the wavenumbers measured with those of the fergusonite and zircon phases it is possible to extrapolate either the high

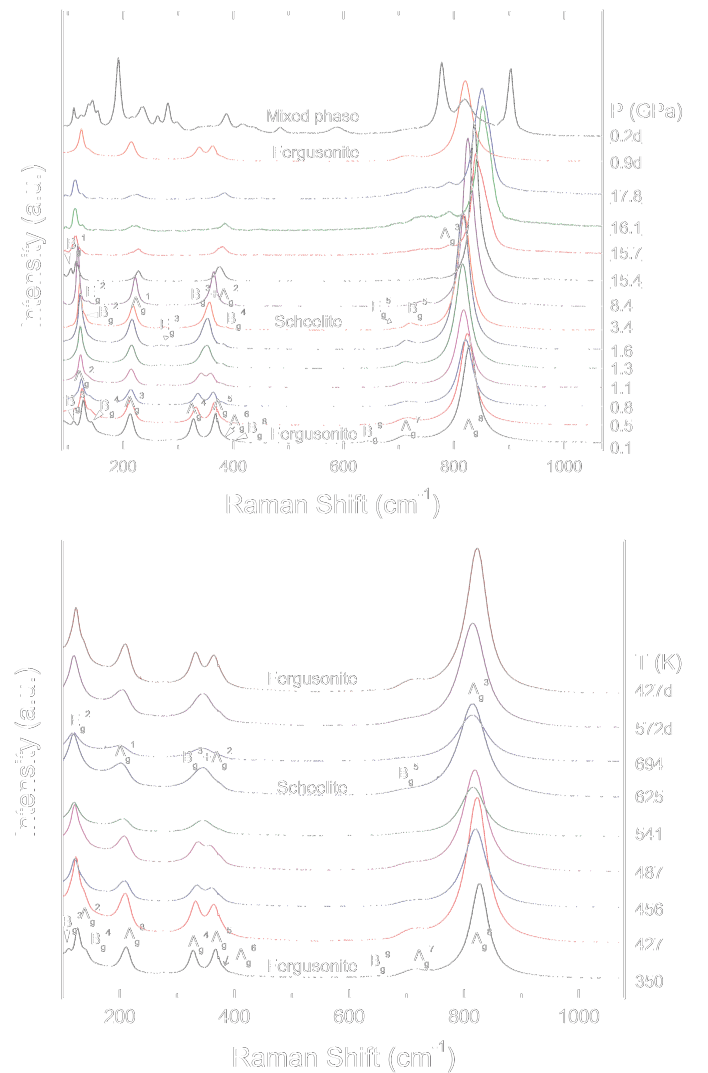


FIG. 2: Raman spectra corresponding to the fergusonite polymorph. Upper panel: selected high pressure spectra. Numbers next to the spectra indicate pressure in GPa, either in the upstroke or downstroke. Spectra correspond to, either different experiments, either with a 16:3:1 methanol:ethanol:water as pressure transmitting medium or *Ne* (underlined pressures) Lower panel: selected spectra at different temperatures (K).

pressure or the high temperature values to ambient conditions. The results are compiled in Tab. II. We observe that both extrapolations agree. High pressure experiments do not involve widening of the modes, as it does happen in high temperature conditions. It is then possible to identify the weakest modes: B_g^2 , E_g^3 , B_g^4 and E_g^5 . Symmetry assignments are based on comparison with *ab initio* calculations, pressure coefficients and correlation between the fergusonite and scheelite phases (see below).

Finally, the Raman active modes in the zircon phase belong to the following representations:

$$\Gamma_R(Z) = 2A_{1g} + 4B_{1g} + B_{2g} + 5E_g \quad (4)$$

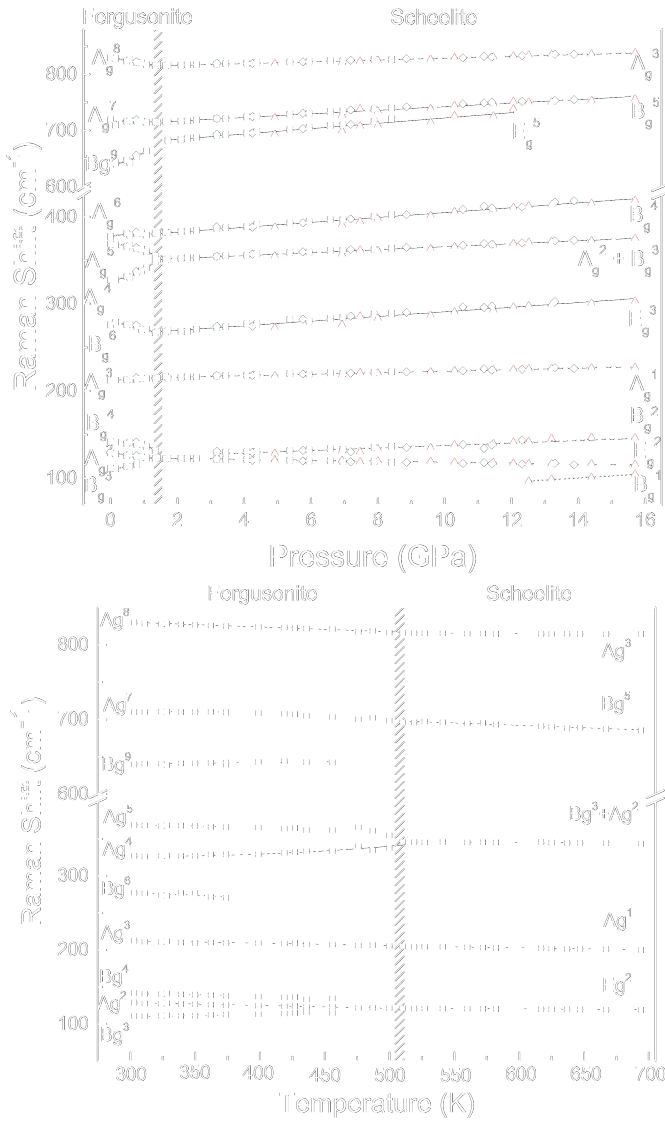


FIG. 3: Upper panel: Pressure dependence of the Raman modes of fergusonite $BiVO_4$. The three different symbols represent three separate experiments. Squares correspond to an experiment in which the sample is in powder form and a 16:3:1 methanol-ethanol-water mixture is used as pressure transmitting medium. Diamonds experiment was carried out with a single crystal and Ne as pressure transmitting medium. Triangles represent an experiment where fergusonite powder and Ne were used. Filled (hollow) symbols were obtained in the upstroke (downstroke). Lower panel: Temperature dependence of the Raman modes of fergusonite structure.

A_{1g} and B_{2g} modes only involve oxygen movements. We present in Fig. 4 the ambient pressure Raman spectrum corresponding to ambient conditions. We have identified 10 out of the 12 modes, as indicated in Tab. III. Compared with previous results,⁶¹ we provided additional information on the weak modes at 194 cm^{-1} (E_g^3) and 429 cm^{-1} (B_{1g}^3). The symmetry assignment has been performed with the aid of *ab initio* calculations. The

TABLE I: Raman frequencies, pressure coefficients and temperature coefficients corresponding to the active Raman modes in the fergusonite structure in ambient conditions. ω is expressed in cm^{-1} , P in GPa and T in K .

Mode	Experimental			Ref. 34	Calculations	
	ω_0	$\partial\omega/\partial P$	$10^3 \cdot \partial\omega/\partial T$	ω_0	ω_0	$\partial\omega/\partial P$
B_g^1				47	43(2)	4.7(2)
B_g^2				55	47(2)	6.1(3)
A_g^1				62	64(3)	-1.2(1)
B_g^3	111(2)	1.2(4)	38(7)	110	123(6)	0.9(1)
A_g^2	129(1)	-4.6(2)	-38(2)	130	136(7)	-2.9(1)
B_g^4	141(1)	-2.1(2)	-42(4)	144	149(7)	-2.3(1)
A_g^3	213(1)	2.0(1)	-32(4)	212	214(11)	0.5(1)
B_g^5	241(1)				250(13)	6.9(3)
B_g^6	276(1)	-2.1(3)	-80(30)	280	278(14)	-1.4(1)
A_g^4	327(1)	3.8(3)	30(30)	326	339(17)	4.8(2)
A_g^5	369(1)	-3.6(2)	-36(8)	370	364(18)	-2.8(1)
A_g^6	383(1)	2.1(2)		386	389(19)	0.9(1)
B_g^7					392(20)	1.3(1)
B_g^8	400(1)			400	400(20)	-0.6(1)
B_g^9	641(1)	7.6(2)	19(4)	642	700(40)	13.0(7)
A_g^7	708(1)	0.2(3)	-9(7)	711	760(40)	5.0(3)
B_{1g}^{10}	747(5)			743	770(40)	-9.0(5)
A_g^8	831(1)	-8.1(3)	-64(2)	830	870(40)	-2.6(1)

TABLE II: Raman frequencies, pressure coefficients and temperature coefficients corresponding to the active Raman modes in the scheelite structure. Wavenumbers have been extrapolated to ambient conditions from high pressure (HP) and high temperature (HT) experiments. ω is expressed in cm^{-1} , P in GPa and T in K .

Mode	Experimental				Calculations	
	ω_0 (HP)	ω_0 (HT)	$\partial\omega/\partial P$	$10^3 \cdot \partial\omega/\partial T$	ω_0	$\partial\omega/\partial P$
E_g^1					19(2)	8.7(4)
B_{1g}^1	67(2)		2.4(2)		32(2)	5.6(3)
B_g^2	124(1)		1.4(1)		127(6)	0.9(1)
E_g^2	124(1)	124(1)	-0.5(1)	-11(1)	141(7)	-0.3(1)
A_g^1	214(1)	211(1)	0.9(1)	-26(1)	219(11)	0.9(1)
E_g^3	265(1)		2.7(1)		256(13)	3.5(2)
A_g^2	349(1)	348(1)	1.7(1)	-9(2)	346(17)	0.9(1)
B_g^3					346(18)	2.7(1)
B_g^4	377(1)		2.8(1)		385(19)	2.0(1)
E_g^4					390(20)	1.3(1)
E_g^5	676(2)		4.7(2)		720(40)	4.1(2)
B_g^5	711(1)	716(4)	3.2(1)	-48(13)	750(40)	3.3(2)
A_g^3	813(1)	817(1)	1.6(1)	-8(1)	850(40)	4.0(2)

agreement between the computed and measured values is within 6 % for most of the modes. In Fig. 4 there is an additional mode marked with a star whose position is close to the most intense peak of the fergusonite phase. We suggest that it is associated to a residual component of the fergusonite phase. As the zircon phase is pure from the point of view of x-ray diffraction, the proportion of the fergusonite phase should be very small (less than 5% approximately).

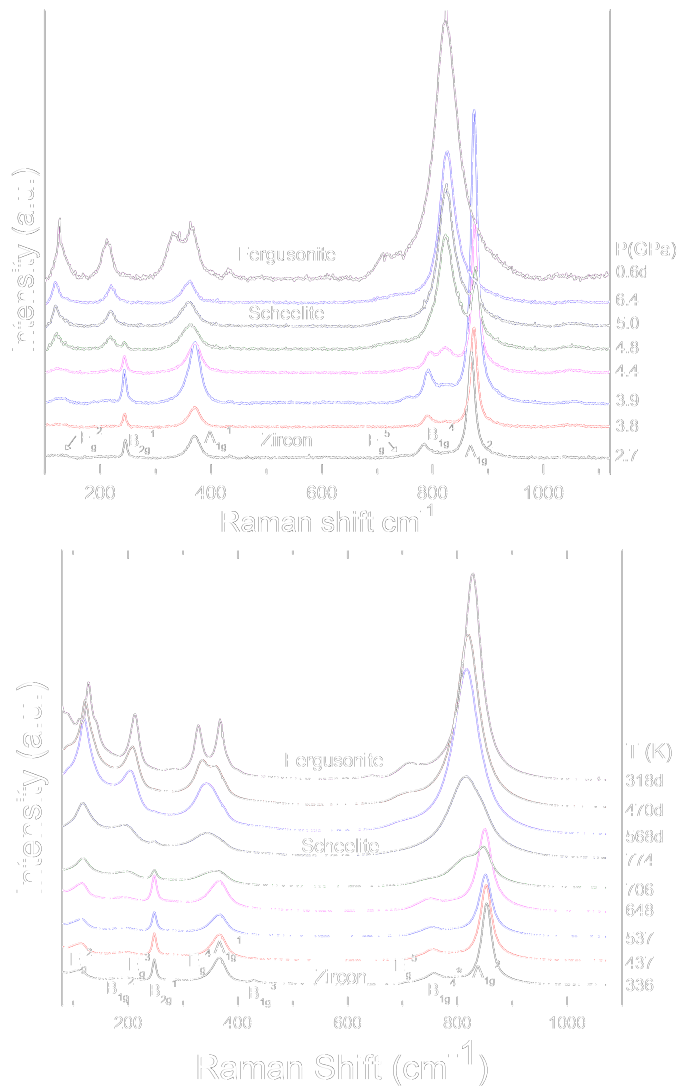


FIG. 4: Raman spectra corresponding to the zircon polymorph. Upper panel: selected high pressure spectra. Numbers next to the spectra indicate pressure in GPa, either in the upstroke or downstroke (d). Methanol-ethanol-water is used as pressure transmitting medium. Lower panel: selected spectra at different temperatures (K).

2. Vibration patterns

Scheelite, fergusonite and zircon structures share structural characteristics.¹¹ The most relevant is the existence of tetrahedral VO_4 units with strong covalent bonds. The O atoms around the Bi atoms define BiO_8 bisdisphenoids which can be visualized as formed by two interpenetrating tetrahedra, one compressed and one elongated. The bisdisphenoids are connected by edges, forming zig-zag chains. The connectivity between the chains and VO_4 tetrahedra differs in scheelite and zircon. Both structures have tetragonal symmetry. However, the packing is not as efficient in the zircon structure as it is scheelite, resulting in a unit cell volume slightly larger

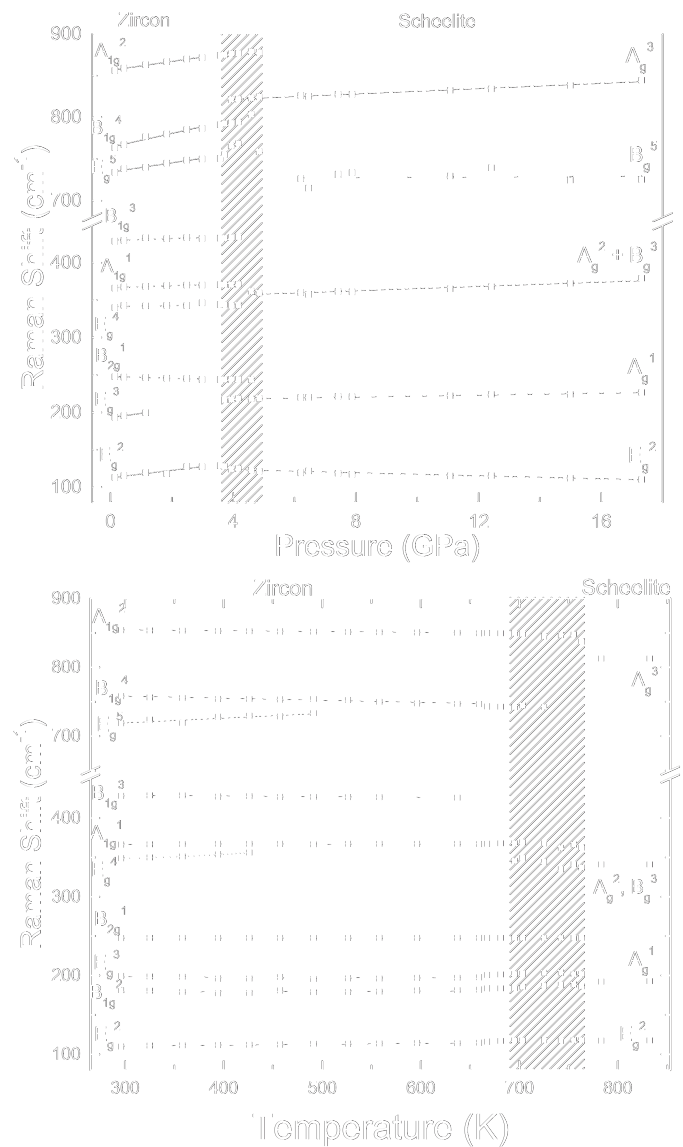


FIG. 5: Raman modes of the zircon polymorph. Upper panel: pressure dependence. Lower panel: temperature dependence.

in zircon than in scheelite. Fergusonite results from the scheelite following a monoclinic distortion associated to the ferroelastic instability. The fergusonite to scheelite transformation is related to a second order phase transition.^{23–25} The reduction in symmetry in fergusonite with respect to scheelite is related to the loss of the four-fold screw axis which implies the following correlations: $A_g, B_g(S) \rightarrow A_g(F)$, $E_g(S) \rightarrow 2B_g(F)$. These correlations are best represented in Fig. 3 by the splitting of the E_g^2 mode into B_g^3 and B_g^4 as well as by the transformation of B_g^5 into A_g^7 or A_g^1 into A_g^3 . On the opposite, the transformation from zircon to scheelite is a first order phase transition implying substantial bond reorganization. Consequently, the modes involved in analogous correlations [$A_{1g}, A_{2g}(Z) \rightarrow A_g(S)$, $B_{1g}, B_{2g}(Z) \rightarrow B_g(S)$, $E_g(Z) \rightarrow E_g(S)$] are affected by discontinuous changes

TABLE III: Raman frequencies, pressure coefficients and temperature coefficients corresponding to the active Raman modes in the zircon structure in ambient conditions. ω is expressed in cm^{-1} , P in GPa and T in K .

Mode	Experimental			Ref. 61	Calculations	
	ω_0	$\partial\omega/\partial P$	$10^3 \cdot \partial\omega/\partial T$	ω_0	ω_0	$\partial\omega/\partial P$
B_{1g}^1					60(3)	3.0(2)
E_g^1					67(3)	3.2(2)
E_g^2	112(2)	5.2(7)	10(2)	113	133(7)	-0.7(1)
B_{2g}^2	179(2)		-30(8)	186	193(10)	2.1(1)
E_g^3	194(1)	3.6(3)	-32(8)		203(10)	3.8(2)
B_{2g}^1	248(1)	-1.1(1)	3(1)	248	269(13)	-1.9(1)
E_g^4	346(3)	0.9(5)	34(6)	348	359(18)	0.6(1)
A_{1g}^1	367(1)	1.2(2)	9(1)	367	366(18)	1.5(1)
B_{2g}^3	429(1)	1.3(7)	-6(7)		440(20)	1.8(1)
E_g^5	734(5)	5.7(6)	80(30)	732	780(40)	4.7(2)
B_{1g}^4	763(6)	8.1(8)	-31(6)	761	810(40)	6.2(3)
A_{2g}^1	857(1)	5.2(3)	-12(1)	856	900(50)	5.4(3)

$$\begin{aligned}
\Gamma_R(S) &= \nu_1(A_g) + \nu_2(A_g) + \nu_2(B_g) + \nu_3(B_g) + \nu_3(E_g) + \nu_4(B_g) + \nu_4(E_g) + T(B_g) + T(E_g) + R(A_g) + R(E_g) + \\
&\quad + Bi(B_g) + Bi(E_g) \\
\Gamma_R(F) &= \nu_1(A_g) + 2\nu_2(A_g) + \nu_3(A_g) + 2\nu_3(B_g) + \nu_4(A_g) + 2\nu_4(B_g) + T(A_g) + 2T(B_g) + R(A_g) + 2R(B_g) + \\
&\quad + Bi(A_g) + 2Bi(B_g) \\
\Gamma_R(Z) &= \nu_1(A_{1g}) + \nu_2(A_{1g}) + \nu_2(B_{2g}) + \nu_3(B_{1g}) + \nu_3(E_g) + \nu_4(B_{1g}) + \nu_4(E_g) + T(B_{1g}) + T(E_g) + R(A_{2g}) + \\
&\quad + R(E_g) + Bi(B_{1g}) + Bi(E_g)
\end{aligned}$$

(5)

The tetrahedra ν_1 mode is only strictly stretching in the zircon and scheelite phases. The A_{1g}^2 mode in zircon (Fig. 6) is the one with the highest frequency (857 cm^{-1}). This is due to the contribution of $Bi-O$ bonds, which in the scheelite A_g^3 (813 cm^{-1}) mode are bent and in zircon are also slightly stretched. In the fergusonite A_g^8 mode (831 cm^{-1}) the $Bi-O$ bonds are also stretched. The frequency decreases with respect to the zircon phase because now the movement of oxygen atoms is not exactly directed along $V-O$ bonds. In zircon and scheelite, only oxygen atoms can vibrate. In fergusonite, V and Bi atoms are allowed to move by symmetry, but the calculation shows that the amplitude of movement is one order of magnitude smaller than that of O atoms.

In scheelite the second highest Raman allowed mode corresponds to B_g^5 (711 cm^{-1}), which is a ν_3 asymmetric stretching bond where V is nearly at rest. $Bi-O$ bonds continue bending. The corresponding mode in fergusonite is the A_g^7 mode (708 cm^{-1}). The vibration pattern is similar to that of scheelite but with the stretching slightly misaligned with respect to the $V-O$ bond. In zircon, the B_{1g}^4 mode (763 cm^{-1}) displays a higher frequency due to the contribution of V atoms to the stretching. The remaining ν_3 mode corresponds to the E_g^5 mode in both scheelite (734 cm^{-1}) and zircon (734 cm^{-1}), Fig. 6. In fergusonite it is related to a couple of modes, B_g^9 (641 cm^{-1}) and B_g^{10} (747 cm^{-1}). In each of

in wavenumber and their relationship is not so clear. In Fig.5 it would seem that $A_{1g}^2 \rightarrow A_g^3$, $B_{1g}^4 \rightarrow B_g^5$, $B_{1g}^3 \rightarrow B_g^3$, $A_{1g}^1 \rightarrow A_g^2$, $B_{2g}^1 \rightarrow B_g^2$, $E_g^2 \rightarrow E_g^2$. The A_g^1 would originate from the silent A_{2g}^1 mode which the calculations situate at 176 cm^{-1} .

As stated above, the three structures share the presence of VO_4 tetrahedra. This fact suggests a discussion of lattice vibrations in terms of modes of the tetrahedra. The internal modes of the tetrahedra (A_1 , E , and $2F_2$) are labelled ν_1 , ν_2 , ν_3 and ν_4 . The rotational (F_1) and translational (F_2) are denoted R and T , respectively, whereas the contribution from Bi atoms are labelled Bi . Considering that there are two tetrahedra and two Bi atoms in each primitive unit cell, the Raman active modes in scheelite and zircon phases can be classified as:

these modes a different pair of O atoms vibrate against the V atom.

The modes appearing in the spectral range between 130 and 450 cm^{-1} are not so readily classifiable in terms of the tetrahedral vibration. The phonon patterns reveal characteristics which can be described as a blend of bending [ν_2 , scissor (ν_4)], translational (T) or rotational modes (R). In the most symmetric zircon structure some of the modes can be identified (Fig. 6): A_{2g}^1 (R , 176 cm^{-1} , silent mode), B_{1g}^2 (T , 179 cm^{-1}), E_g^4 (ν_4 , 346 cm^{-1}) and A_{1g}^1 (ν_2 , 367 cm^{-1}).

The least energetic modes are the only ones in which Bi atoms vibrate with non negligible amplitudes. In zircon, Bi atoms vibrate along the c -axis in B_{1g}^1 (60 cm^{-1}) or in the perpendicular direction, as in E_g^1 (67 cm^{-1}). Bi atoms connected by glide planes shift in opposite directions. V atoms are at rest. In scheelite, Bi atoms vibrate along the c axis in the B_g^1 mode. Bi atoms and V atoms with the same x and y atomic coordinate shift in the same direction. In the E_g^1 mode Bi atoms have a large amplitude in the direction perpendicular to the c -axis. The amplitude of V and O atoms is one order of magnitude smaller. In fergusonite, the B_g^1 and B_g^2 (43 and 47 cm^{-1}) modes display Bi movement perpendicular to the binary axis, whereas in the A_g^1 (62 cm^{-1}) mode the movement is along the binary axis. V atoms only move in B_g^1 .

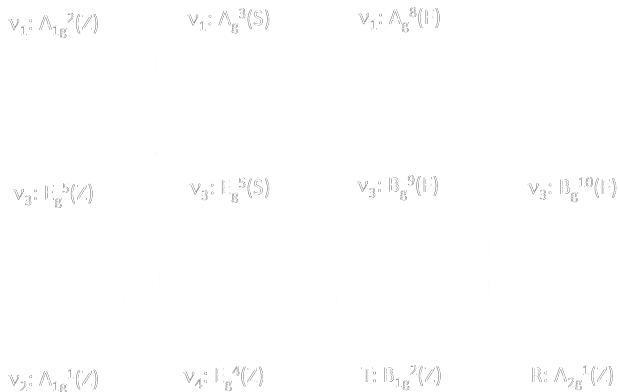


FIG. 6: . Selected patterns of lattice vibrations at the gamma point in zircon (Z), scheelite (S) and fergusonite (F). Large, medium and small spheres represent *Bi*, *V* and *O* atoms, respectively. We represent only the first neighbor cell of *V* and *Bi* atoms. Modes labelled ν , T and R are derived from the internal, translational and rotational modes of the VO_4 tetrahedra.

B. High pressure and high temperature studies

C. Pressure and temperature coefficients

We focus first on pressure and temperature coefficients. The wavenumber dependence is linear in scheelite, slightly differs from linearity in zircon and is more complex in the fergusonite structure. The coefficients presented in Tabs. I and III have been obtained using data obtained near ambient conditions, where the dependence either in pressure or temperature is linear. The data of the pressure coefficients largely coincide with those obtained with *ab initio* calculations, in both value and the sign. Only the pressure coefficients associated with the E_g^2 mode of the zircon phase and the B_g^9 , A_g^7 and A_g^8 modes of the fergusonite phase differ significantly from the coefficients obtained from the simulation. In Ref. 24, high pressure and high temperature x-ray diffraction studies are compared plotting the lattice parameters as a function of volume, concluding that lattice axes depend linearly on relative volume, independent of temperature or pressure. If this is the case, and harmonic effects prevail, signs in pressure and temperature coefficients should be opposite. This is in fact what is observed in the scheelite structure. In the zircon polymorph nearly half of the modes follow this rule, whereas in fergusonite nearly all of them show pressure and temperature coeffi-

cients with the same sign. We conclude that anharmonic effects determine decisively the lattice dynamics in the fergusonite structure, they are also present in the zircon structure but they are not evident in the scheelite structure. Anharmonic effects will be further discussed in Sec. IV E.

D. Phase transitions

Fig.2 presents the evolution of Raman spectra of fergusonite $BiVO_4$ under high pressure (upper panel) or temperature (lower panel). Merging of A_g^4 and A_g^5 modes on the one hand and B_g^3 , A_g^2 and B_g^4 on the other, is readily appreciable when pressure or temperature increases, up to the fergusonite to scheelite phase transition. When extreme conditions are relaxed, the sample reverts to the fergusonite structure. The wavenumbers measured in the downstroke or on cooling do not show any hysteresis (void symbols in Fig.3), in agreement with the reversible character of the phase transition.^{24,27,29} From combined high pressure-high temperature experiments (not shown), we determine the boundary of the fergusonite to scheelite phase transition as given by:

$$T_{F-Sch} = -166(8) * P + 528(5), \quad (6)$$

where temperature is in GPa and T in K . As a comparison, the boundary is given by $T_{F-Sch} = -150(8) * P + 523(3)$ following Ref. 27 or $dT_{F-Sch}/dP = -166(8)$ in Ref. 26.

Fig.4 shows the behavior of Raman spectra of zircon $BiVO_4$ from 0 to 6.4 GPa (upper panel) and from room temperature to 774 K (lower panel). In both cases the emergence of the A_g^3 (213 cm^{-1}) and A_g^8 (831 cm^{-1}) modes indicates the transition to the scheelite structure. The phase transition is gradual. The range of pressure/temperature values where both phases coexist has been greyed in Fig. 5. Using as a criteria the destabilization of the zircon structure, as indicated by the appearance of the first fergusonite peaks in combined high pressure-high temperature experiments (not shown), the phase transition boundary is determined to be:

$$T_{Z-Sch} = -107(8) * P + 690(10), \quad (7)$$

The transition from the zircon to the scheelite phase was determined²² to range between 673 to 773 K by combined differential thermal analysis (DTA) and XRD of quenched samples. Subsequent⁴² DTA studies yielded temperatures between 623 and 723 K. Up to our knowledge, there are not previous studies on the high pressure stability of zircon $BiVO_4$. However, there has been a lot of work on the high pressure behaviour of other zircon orthovanadates. The transition pressure from the zircon to the scheelite⁶² structure is always a few gigapascals.

The range of stability of the scheelite phase is small. In Fig. 2 we show spectra corresponding to higher pressures. At 15.7 GPa new modes appear. The A_g^1 mode is doubled. The sample becomes very inhomogeneous, as qualitatively different spectra are measured in different parts of the sample. From Raman studies alone we cannot discard sample decomposition. This behaviour has been observed irrespectively of the pressure transmitting medium employed (MEW or Ne), sample form (powder or single crystal) or initial crystalline structure (fergusonite or zircon). The destabilization of the scheelite phase is observed at lower pressures (13.8 GPa) if less hydrostatic pressure transmitting media are used (MEW). The changes observed are irreversible, being the spectrum recovered from 17.8 GPa different from the initial fergusonite phase.

E. Order parameter

We have pointed out in Sec. IV C the strong anharmonic behaviour of lattice modes of the fergusonite structure as revealed by the sign of pressure and temperature coefficients. We are going now to deepen the relationship between the anharmonic behaviour of the modes and the static distortion which stabilizes the monoclinic distortion. According to lattice dynamical theory,⁶³ the anharmonic coupling (quantified by α_k) of any phonon (wavenumber ω_k) with the order parameter (η) results in a modification of the phonon wavenumber given by $\tilde{\omega}_k^2 = \omega_k^2 + 1/2\alpha_k\eta^2$.

We have also seen in Sec. IV A 2 that the Eg_2 mode in scheelite gives raise to the B_g^3 and B_g^4 modes in fergusonite. In absence of the static distortion both modes would have the same wavenumber. We can write then:

$$\eta = \frac{2(\omega_{B_g^4}^2 - \omega_{B_g^3}^2)}{\alpha_{B_g^4} - \alpha_{B_g^3}} \quad (8)$$

The pressure and temperature behaviour of A_g^5 and A_g^6 modes is also clearly correlated. However, in this case they do not originate from a doublet mode in scheelite, but from B_g^3 and A_g^2 modes, which are accidentally degenerated. It seems reasonable to assume that without the anharmonic interaction they would continue to be degenerated. We can approximate:

$$\eta \simeq \frac{2(\omega_{A_g^6}^2 - \omega_{A_g^5}^2)}{\alpha_{A_g^6} - \alpha_{A_g^5}} \quad (9)$$

The free energy can be written⁶³ as a Landau expansion as:

$$F(\eta) = F(0) + \frac{1}{2}A(T - T_c)\eta^2 + \frac{1}{4}B\eta^4, \quad (10)$$

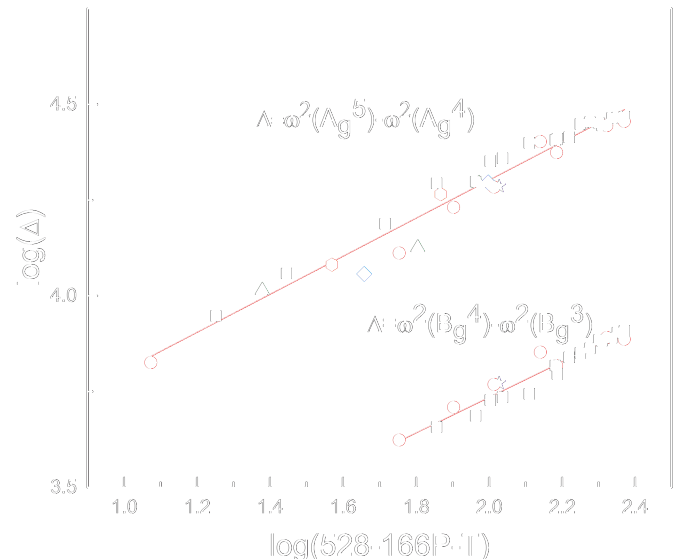


FIG. 7: Analysis of the order parameter as pressure and/or temperature is varied. Δ is proportional to the order parameter (Eqns. 8 and 9). Pressure and temperature are combined as in Eqn. 6. Symbols correspond to different experiments. Squares: ambient pressure, temperature variation; circles: ambient temperature, pressure variation; triangles: $T=331$ K, pressure variation; rhombs: $T=342$ K, pressure variation; hexagons: $T=391$ K, pressure variation.

where A and B are constants and T_c is considered to depend on both pressure and temperature as given in Eqn. 6. Minimizing the free energy leads to an alternate expression of the order parameter:

$$\eta = \sqrt{\frac{A}{B}(T_c[T, P] - T)} \quad (11)$$

Fig. 7 tests the theory just described comparing either Eq. 8 or 9 with Eq. 11, in the whole set of high pressure-high temperature experiments performed. The linear fits displayed in Fig. 7 are described by: $\log[\Delta(A_g^5 - A_g^4)] = 0.50(2)(T_c(P) - T) + 3.31(4)$, $\log[\Delta(B_g^4 - B_g^3)] = 0.46(4)(T_c(P) - T) + 2.81(5)$. The critical exponent of the fergusonite to scheelite phase transition is then 1/2, as expected in a second order phase transition.

V. CONCLUSIONS

We have discussed eleven Raman experiments, corresponding to three $BiVO_4$ polymorphs, fergusonite, scheelite and zircon; under high pressure, high temperature or a combination of both. Our results are interpreted with the aid of *ab initio* calculations.

We determine the wavenumbers of previously uncharacterized modes of the three phases. The modes of the three structures are related based not only in their symmetry but also on their relationship with the VO_4 tetra-

hedra. *Ab initio* calculations provide the phonon patterns, which were not available in the literature.

High pressure and high temperature studies reveal a qualitatively different behaviour of the three phases. Pressure and temperature induce a linear shift of wavenumbers in scheelite. In the zircon phase the shift is slightly non linear, whereas in the fergusonite phase it is more complex. We determine pressure and temperature coefficients for the three phases. The behaviour of the fergusonite phase is decisively affected by anharmonic effects, which are evidenced by the sign of their pressure and temperature coefficients. We have analyzed the anharmonic contribution to the wavenumber shift using an order parameter. The introduction of a critical temperature depending both on temperature and pressure allows the description of the results of all the experiments in a unified way.

Fergusonite transforms to the scheelite phase under high pressure or high temperature. The phase transition boundary is given by eqn. 6. It is a reversible second order phase transition. We have shown that the critical exponent associated to the transition is $1/2$. Zircon also transform to the scheelite phase under high pressure or temperature, but this time the transition is first order and irreversible. The zircon phase is destabilized at

pressures and temperatures given by eqn. 7. The scheelite phase is stable up to 15.7 GPa . The modifications observed in the spectra are partially retained when high pressure is released.

Acknowledgments

This work has been supported by Ministerio de Ciencia e Innovación of Spain (MICINN) under The National Program of Materials (MAT2013-46649-C4-1-P, MAT2016-75586-C4-1-P/3-P) and The Consolider-Ingenio 2010 Program (MALTA CSD2007-0045) and by the EU-FEDER funds. D. Vázquez wishes to thank MICINN for the FPI grant (BES-2014-068953). A. J. E. Rettie and C. B. Mullins thank the Welch Foundation (F-1436) and the U. S. Department of Energy Basic Energy Sciences (grant DE-FG02-09ER16119) for their generous support. S. L.-M. thanks CONACYT of México for financial support through the program "Catedras para Jóvenes Investigadores". Also, some of the computing for this project was performed with the resources of the IPICYT Supercomputing National Center for Education & Research, grant TKII-R2018-SLM1.

* Electronic address: Julio.Pellicer@uv.es

- ¹ W. Ryba-Romanowski, *Crystal Research and Technology* **38**, 225 (2003).
- ² S. Miyazawa, *Opto-Electronics Review* **11**, 77 (2003).
- ³ M. Oshikiri, M. Boero, A. Matsushita, and J. Ye, *The Journal of Chemical Physics* **131**, 034701 (2009).
- ⁴ K. Fukudome, N.-o. Ikenaga, T. Miyake, and T. Suzuki, *Catal. Sci. Technol.* **1**, 987 (2011).
- ⁵ C.-J. Jia, L.-D. Sun, F. Luo, X.-C. Jiang, L.-H. Wei, and C.-H. Yan, *Applied Physics Letters* **84**, 5305 (2004).
- ⁶ A. A. Kaminskii, H. Rhee, H. J. Eichler, K. Ueda, K. Oka, and H. Shibata, *Applied Physics B* **93**, 865 (2008).
- ⁷ A. A. Kaminskii, O. Lux, H. Rhee, H. J. Eichler, K. Ueda, H. Yoneda, A. Shirakawa, B. Zhao, J. Chen, J. Dong, et al., *Laser Physics Letters* **9**, 879 (2012).
- ⁸ C. M. Suarez, S. Hernández, and N. Russo, *Applied Catalysis A: General* **504**, 158 (2015).
- ⁹ Q. Jia, K. Iwashina, and A. Kudo, *Proceedings of the National Academy of Sciences* **109**, 11564 (2012).
- ¹⁰ A. Kudo, K. Omori, and H. Kato, *Journal of the American Chemical Society* **121**, 11459 (1999).
- ¹¹ R. J. Finch and J. M. Hanchar, *Reviews in Mineralogy and Geochemistry* **53**, 1 (2003).
- ¹² N. Clavier, R. Podor, and N. Dacheux, *Journal of the European Ceramic Society* **31**, 941 (2011).
- ¹³ V. Panchal, D. Errandonea, F. J. Manjón, A. Muñoz, P. Rodríguez-Hernández, M. Bettinelli, S. N. Achary, and A. K. Tyagi, *AIP Conference Proceedings* **1665**, 030006 (2015).
- ¹⁴ V. Panchal, S. López-Moreno, D. Santamaría-Pérez, D. Errandonea, F. J. Manjón, P. Rodríguez-Hernández, A. Muñoz, S. N. Achary, and A. K. Tyagi, *Phys. Rev. B*

84, 024111 (2011).

- ¹⁵ D. Errandonea, R. S. Kumar, S. N. Achary, and A. K. Tyagi, *Phys. Rev. B* **84**, 224121 (2011).
- ¹⁶ V. Panchal, D. Errandonea, A. Segura, P. Rodríguez-Hernández, A. Muñoz, S. Lopez-Moreno, and M. Bettinelli, *Journal of Applied Physics* **110**, 043723 (2011).
- ¹⁷ D. Errandonea, S. N. Achary, J. Pellicer-Porres, and A. K. Tyagi, *Inorganic Chemistry* **52**, 5464 (2013).
- ¹⁸ A. B. Garg, D. Errandonea, P. Rodríguez-Hernández, S. López-Moreno, A. Muñoz, and C. Popescu, *Journal of Physics: Condensed Matter* **26**, 265402 (2014).
- ¹⁹ D. Garg, A. B. and Errandonea, *Journal of Solid State Chemistry* **226**, 147 (2015), ISSN 0022-4596.
- ²⁰ B. Yue, F. Hong, S. Merkel, D. Tan, J. Yan, B. Chen, and H.-K. Mao, *Phys. Rev. Lett.* **117**, 135701 (2016).
- ²¹ G. Dreyer and E. Tillmanns, *Neues Jahrbuch Fur Mineralogie-Monatshefte* pp. 151–154 (1981).
- ²² R. S. Roth and J. L. Waring, *American Mineralogist* **48**, 1348 (1963).
- ²³ A. Sleight, H. y. Chen, A. Ferretti, and D. Cox, *Materials Research Bulletin* **14**, 1571 (1979).
- ²⁴ J. W. E. Mariathasan, R. M. Hazen, and L. W. Finger, *Phase Transitions* **6**, 165 (1986).
- ²⁵ J. Bierlein and A. Sleight, *Solid State Communications* **16**, 69 (1975).
- ²⁶ A. Pinczuk, B. Welber, and F. Dacol, *Solid State Communications* **29**, 515 (1979).
- ²⁷ R. M. Hazen and J. W. E. Mariathasan, *Science* **216**, 991 (1982).
- ²⁸ I. G. Wood, B. Welber, W. I. F. David, and A. M. Glazer, *Journal of Applied Crystallography* **13**, 224 (1980).
- ²⁹ W. I. F. David, A. M. Glazer, and A. W. Hewat, *Phase*

- Transitions **1**, 155 (1979).
- ³⁰ A. Pinczuk, G. Burns, and F. Dacol, *Solid State Communications* **24**, 163 (1977).
- ³¹ H. Tokumoto and H. Unoki, *Phys. Rev. B* **27**, 3748 (1983).
- ³² G. Benyuan, M. Copic, and H. Z. Cummins, *Phys. Rev. B* **24**, 4098 (1981).
- ³³ I. Tomeno, N. Sato, Y. Sato, K. Oka, and Y. Tsunoda, *Phys. Rev. B* **84**, 014302 (2011).
- ³⁴ L. P. Avakyants, A. V. Chervyakov, V. S. Gorelik, and P. P. Sverbil', *Journal of Russian Laser Research* **25**, 535 (2004).
- ³⁵ S. Segel, *Solid State Communications* **54**, 403 (1985).
- ³⁶ A. Sleight, K. Aykan, and D. Rogers, *Journal of Solid State Chemistry* **13**, 231 (1975).
- ³⁷ H. S. Park, K. E. Kweon, H. Ye, E. Paek, G. S. Hwang, and A. J. Bard, *The Journal of Physical Chemistry C* **115**, 17870 (2011).
- ³⁸ S. P. Berglund, A. J. E. Rettie, S. Hoang, and C. B. Mullins, *Phys. Chem. Chem. Phys.* **14**, 7065 (2012).
- ³⁹ M. M. Qurashi and W. H. Barnes, *American Mineralogist* **5**, 489 (1953).
- ⁴⁰ A. J. E. Rettie, H. C. Lee, L. G. Marshall, J.-F. Lin, C. Capan, J. Lindemuth, J. S. McCloy, J. Zhou, A. J. Bard, and C. B. Mullins, *Journal of the American Chemical Society* **135**, 11389 (2013).
- ⁴¹ A. J. E. Rettie, W. D. Chemelewski, J. Lindemuth, J. S. McCloy, L. G. Marshall, J. Zhou, D. Emin, and C. B. Mullins, *Applied Physics Letters* **106**, 022106 (2015).
- ⁴² A. Bhattacharya, K. Mallick, and A. Hartridge, *Materials Letters* **30**, 7 (1997).
- ⁴³ S. Klotz, J.-C. Chervin, P. Munsch, and G. L. Marchand, *Journal of Physics D: Applied Physics* **42**, 075413 (2009).
- ⁴⁴ H. Mao, J. Xu, and P. Bell, *J. Geophys. Res.* **91**, 4673 (1986).
- ⁴⁵ F. Datchi, R. LeToullec, and P. Loubeyre, *J. Appl. Phys.* **81**(8), 3333 (1997).
- ⁴⁶ R. O. Jones, *Rev. Mod. Phys.* **87**, 897 (2015).
- ⁴⁷ P. E. Blöchl, *Phys. Rev. B* **50**, 17953 (1994).
- ⁴⁸ G. Kresse and D. Joubert, *Phys. Rev. B* **59**, 1758 (1999).
- ⁴⁹ G. Kresse and J. Hafner, *Phys. Rev. B* **47**, 558 (1993).
- ⁵⁰ G. Kresse and J. Hafner, *Phys. Rev. B* **49**, 14251 (1994).
- ⁵¹ G. Kresse and J. Furthmüller, *Phys. Rev. B* **54**, 11169 (1996).
- ⁵² G. Kresse and J. Furthmüller, *Computational Materials Science* **6**, 15 (1996), ISSN 0927-0256.
- ⁵³ J. Heyd, G. E. Scuseria, and M. Ernzerhof, *The Journal of Chemical Physics* **118**, 8207 (2003).
- ⁵⁴ J. Heyd and G. E. Scuseria, *The Journal of Chemical Physics* **121**, 1187 (2004).
- ⁵⁵ J. Paier, M. Marsman, K. Hummer, G. Kresse, I. C. Gerber, and J. G. Ángyán, *The Journal of Chemical Physics* **124**, 154709 (2006).
- ⁵⁶ J. Heyd, G. E. Scuseria, and M. Ernzerhof, *The Journal of Chemical Physics* **124**, 219906 (2006).
- ⁵⁷ S. López-Moreno, P. Rodríguez-Hernández, A. Muñoz, and D. Errandonea, *Inorganic Chemistry* **56**, 2697 (2017).
- ⁵⁸ S. López-Moreno, D. Errandonea, J. Pellicer-Porres, D. Martínez-García, S. J. Patwe, S. N. Achary, A. K. Tyagi, P. Rodríguez-Hernández, A. Muñoz, and C. Popescu, *Inorganic Chemistry* **57**, 7860 (2018).
- ⁵⁹ H. J. Monkhorst and J. D. Pack, *Phys. Rev. B* **13**, 5188 (1976).
- ⁶⁰ K. Parlinski, *Computer code phonon*, <http://wolf.ifj.edu.pl/phonon>.
- ⁶¹ J. Yi, Z. Zhao, Y. Wang, D. Zhou, C. Ma, Y. Cao, and J. Qiu, *Materials Research Bulletin* **57**, 306 (2014).
- ⁶² D. Errandonea and A. B. Garg, *Progress in Materials Science* **97**, 123 (2018).
- ⁶³ M. T. Dove, *Structure and Dynamics*, Oxford Master Series in Condensed Matter Physics (Oxford University Press, 2003).